

Supermassive primordial black holes: A view from clustering of quasars at $z \sim 6$

Takumi Shinohara,¹ Wanqiu He,² Yoshiki Matsuoka,³ Tohru Nagao,³ Teruaki Suyama,⁴ and Tomo Takahashi⁵

¹*Graduate School of Science and Engineering, Saga University, Saga 840-8502, Japan*

²*National Astronomical Observatory of Japan, 2-21-1 Osawa, Mitaka, Tokyo 181-8588, Japan*

³*Research Center for Space and Cosmic Evolution, Ehime University, Matsuyama, Ehime 790-8577, Japan*

⁴*Department of Physics, Tokyo Institute of Technology, 2-12-1 Ookayama, Meguro-ku, Tokyo 152-8551, Japan*

⁵*Department of Physics, Saga University, Saga 840-8502, Japan*



(Received 14 April 2023; accepted 15 August 2023; published 12 September 2023)

We investigate a scenario where primordial black holes (PBHs) can be the progenitors of supermassive black holes (SMBHs) observed at $z \sim 6$. To this end, we carried out clustering analysis using a sample of 81 quasars at $5.88 < z < 6.49$, which is constructed in the Subaru High- z Exploration of Low-Luminosity Quasars project, and 11 quasars in the same redshift range selected from the literature. The resulting angular autocorrelation function (ACF) can be fitted to a power law form of $\omega_\theta = 0.045_{-0.106}^{+0.114} \theta^{-0.8}$ over a scale of 0.2–10 degrees. We compare the ACF of the quasars to that predicted for the PBH model at $z \sim 6$ and found that such a scenario is excluded for a broad range of parameter space, from which we can conclude that a scenario with PBHs as SMBHs is not viable. We also discuss a model in which SMBHs at $z \sim 6$ originate from the direct collapse of PBH clumps and argue that the observed ACF excludes such a scenario in the context of our PBH model.

DOI: [10.1103/PhysRevD.108.063510](https://doi.org/10.1103/PhysRevD.108.063510)

I. INTRODUCTION

Observational wide-field optical and near-infrared surveys such as the Sloan Digital Sky Survey [1,2], the Subaru High- z Exploration of Low-Luminosity Quasars (SHELLQs) [3–5], the Canada-France-Hawaii Telescope Legacy Survey [6,7], the Panoramic Survey Telescope and Rapid Response System 1 [8], and the United Kingdom Infrared Telescope Infrared Deep Sky Survey [9] have discovered quasars powered by supermassive black holes (SMBHs) at redshift around and higher than 6. The virial black hole mass estimated from their single-epoch spectra suggest that the mass of SMBHs in such high- z quasars had been already grown up to $\sim 10^8$ – $10^{10} M_\odot$ even when the age of the Universe was less than 1 Gyr (e.g., [10–12]). However, the formation of SMBHs at high redshift from astrophysical processes is a challenging task and a lot of efforts have been made to understand the mechanism (for a review, see, e.g., [13]).

Another avenue to explain SMBHs at high- z is primordial black holes (PBHs) [14–17] as a progenitor, which has been attracting attention in cosmology. Indeed PBHs have been a target of intense study since it can explain dark matter of the Universe for some mass range [18] and the gravitational wave signals detected by LIGO [19–21]. An advantage of considering PBHs as the origin of SMBHs is that the initial mass of PBHs is specified by the

characteristic comoving wave number that is a free parameter characterizing the primordial power spectrum and it is possible to produce PBHs whose initial mass is in the mass range $10^8 M_\odot$ – $10^{10} M_\odot$ by simply adopting appropriate value of the comoving wave number [see Eq. (2.1)], which is in sharp contrast with the Pop-III scenario for which an additional astrophysical process to achieve efficient mass growth from initial masses $\lesssim 10^3 M_\odot$ is needed [22–24].¹ On the other hand, a nontrivial issue is that a significant enhancement of the primordial power spectrum from the standard power-law form with the spectral index $n_s \approx 0.96$ must occur at small scales to realize the $\mathcal{O}(1)$ amplitude of the primordial curvature perturbations required for the PBH formation, as it is argued in [29]. A possibility that PBHs play a role of SMBHs has been discussed in the context of some concrete models in [30–34].

Although the direct formation of the SMBHs is an appealing feature of the PBH scenario, it is logically possible that PBHs are formed with their initial masses $\lesssim 10^3 M_\odot$ and grow to SMBHs until the redshifts of observations. Yet, there is no strong motivation to consider this possibility since Pop-III stars can be such initial seed

¹It has also been discussed that supermassive stars with $\sim 10^5 M_\odot$ or the collapse of massive gas clouds can also produce sufficiently massive seed black holes (see, e.g., [25–28]).

BHs. Thus, except the last paragraph in Sec. IV, throughout this paper, we assume that initial PBH masses are in the mass range $10^4 M_\odot - 10^{10} M_\odot$.²

It is known that PBH formation in the mass range $10^4 M_\odot - 10^{10} M_\odot$ contradicts with nondetection of the spectral distortion of cosmic microwave background (CMB) if such PBHs are produced from Gaussian primordial fluctuations [35]. Therefore one needs to invoke a highly non-Gaussian perturbation to successfully produce PBHs as SMBHs without conflicting with this constraint. One natural path to realize such a scenario is to introduce a light spectator field whose fluctuations produced during inflation source the non-Gaussian curvature perturbation at late epoch.³ This idea has been framed in concrete models in [31–34]. Recently, in [37], three of the present authors have shown that the distribution of PBHs is highly clustered in such models by explicitly demonstrating that the computed angular correlation function of PBHs becomes large over a wide range of angles (see also [38]). Since the essence of the clustering comes from the modulation of the local amplitude of the perturbation (at the scales corresponding to the PBH formation) caused by the superposition of the long-wavelength modes, the strong clustering of PBHs is a generic feature in the light spectator field models.⁴

Although it was suggested in [37] that large amplitude of the angular correlation function is likely to be incompatible with the observed quasars, a definite conclusion was not drawn because the angular correlation function (ACF) predicted in the model was not confronted with observational data. This paper continues forward by comparing the angular correlation function computed in [37] with actual observational data as a critical test for the PBH scenario as SMBHs. To this end, we derive the angular correlation function for quasars at $5.88 < z < 6.49$ discovered in SHELLQs project, and additional quasars in the same redshift range detected in the literature [42]. Then we compare the ACF of quasars with that of PBHs, which is predicted [37], and show that most parameter space are likely to be excluded by the observational result. In particular, the case where the mass of the spectator field is much smaller than the Hubble parameter during inflation

²For the PBH mass of $\lesssim 10^8 M_\odot$, some astrophysical process such as accretion is required so that PBHs grow to obtain observed masses of SMBHs.

³Recent work [36] proposed a new scenario based on multi-field inflation models where bubbles formed through the tunneling process during inflation can lead to PBHs, which does not make use of the standard quantum fluctuations of fields produced during inflation. In this scenario, CMB spectral distortion is not induced. Furthermore, if the isocurvature modes are heavy, then the tunneling rate will depend only on the adiabatic direction. In such a case, the spatial distribution of PBHs will obey the Poisson distribution.

⁴In general, when short-wavelength perturbations are modulated by the long-wavelength perturbations by the presence of local non-Gaussianity, the resultant PBHs are clustered [39–41].

is rejected. Therefore, as we argue in this paper, we can conclude that PBH models based on the light spectator field as a progenitor of SMBHs are not viable.

This paper is organized as follows. In Sec. II, we briefly summarize our model to derive the clustering of PBHs at $z \sim 6$. In Sec. III, we introduce the quasar sample used for clustering analysis in this study and evaluate the clustering of quasars at $z \sim 6$ via the ACF. Then the comparison between the two ACFs and the constraints on model parameter space are discussed in Sec. IV. We give conclusions in the final section.

II. PBHs AS SMBHs

In this section, based on Ref. [37], we first give a brief overview of the scenario that explains the existence of the SMBHs at redshifts around $z = 6$ as a result of formation of PBHs in the very early Universe. After that, we briefly give a formalism to evaluate the angular correlation function of PBHs that we compare with observational data of quasars at $z \sim 6$.

A PBH is formed when the primordial density perturbation that has a density contrast of $\mathcal{O}(1)$ amplitude reenters the Hubble horizon [15]. Crudely speaking, the initial PBH mass M_{PBH} is equal to the horizon mass evaluated at the time of the horizon reentry, which gives a relation between the (comoving) wave number k of the perturbation and M_{PBH} as

$$k \sim 100 \text{ Mpc}^{-1} \left(\frac{M_{\text{PBH}}}{10^{10} M_\odot} \right)^{-1/2}. \quad (2.1)$$

Such a large-amplitude perturbation must be very rare, otherwise the SMBHs are overproduced and the Universe would be dominated soon after their formation,⁵ which is not compatible with reality. If the primordial perturbations of the mode with wave number k corresponding to $10^4 M_\odot \lesssim M_{\text{PBH}} \lesssim 10^{10} M_\odot$ are Gaussian/nearly Gaussian, then it is known that such perturbations lead to a sizable CMB spectral distortion incompatible with the nondetection of such distortion in the CMB experiment [35]. Therefore, the primordial perturbations that can explain the abundance of the observed SMBHs at high redshifts and, at the same time, produce little CMB spectral distortion must be strongly non-Gaussian.

Such non-Gaussian primordial perturbations may be naturally realized by the quantum fluctuations of the spectator field created during inflation. The spectator field is a scalar field which acquires quantum fluctuations during inflation but is not an inflaton and subdominant during inflation. Approximating the spectator field as a free field, the fluctuations of the spectator field are Gaussian. However,

⁵The formation time of PBH with its mass M_{PBH} is $t \sim 10^5 \text{ s} \left(\frac{M_{\text{PBH}}}{10^{10} M_\odot} \right)$.

thanks to the subdominance of the spectator field, it is possible to build a model where the primordial perturbations generated from the spectator field fluctuations become highly non-Gaussian. In such a case, production of PBHs occurs at locations corresponding to the extremely high-sigma peaks of the spectator field fluctuations while suppressing the CMB spectral distortion at a level much below the upper limit set by the existing CMB experiment. This production mechanism of PBHs have also been considered and studied in [31–34,43]. A characteristic prediction common to all the concrete models studied in these papers is the strong clustering of the PBHs. This feature is due to the fact that the rarer the peaks of the Gaussian fluctuations are, the more such peaks are spatially clustered [44].

The angular correlation function of PBHs originating from the spectator field fluctuations explained above has been computed in [37] under the assumptions that (i) PBHs do not grow substantially by accretion between the time of formation and the observation time (i.e., $z \sim 6$)⁶ and (ii) the time evolution of the PBH correlation function due to mergers and motions of PBHs is negligible for the scales probed by the observations. According to [37], the angular correlation function of PBHs existing between the redshift range $z_{\text{low}} < z < z_{\text{high}}$ is given by

$$w_{\text{PBH}}(\theta) = \int_{R_{\text{low}}}^{R_{\text{high}}} dR_1 \int_{R_{\text{low}}}^{R_{\text{high}}} dR_2 \frac{3R_1^2}{R_{\text{high}}^3 - R_{\text{low}}^3} \times \frac{3R_2^2}{R_{\text{high}}^3 - R_{\text{low}}^3} \xi_{\text{PBH}}(R_1, R_2, \theta). \quad (2.2)$$

Here, $R_{\text{low}} \equiv R(z_{\text{low}})$ and $R_{\text{high}} \equiv R(z_{\text{high}})$ are the comoving distance $R(z) \equiv \int_0^z \frac{dz'}{H(z')}$ for $z = z_{\text{low}}$ and $z = z_{\text{high}}$, respectively, and ξ_{PBH} is the correlation function of PBHs given by

$$\xi_{\text{PBH}}(r) \approx \frac{(1 + \epsilon(r))^{\frac{3}{2}}}{\sqrt{1 - \epsilon(r)}} \exp\left(\frac{\epsilon(r)\nu^2}{1 + \epsilon(r)}\right) - 1. \quad (2.3)$$

⁶Inclusion of the effect of mass growth of PBHs due to accretion amounts to taking smaller value of M_{PBH} in Eq. (2.1). In [37], it was shown that any choice of M_{PBH} in the range $10^4 M_{\odot} \lesssim M_{\text{PBH}} \lesssim 10^{10} M_{\odot}$ predicts a very large amplitude of the PBH correlation function whose shape depends on its mass and the parameters in the model, but the size does not change qualitatively, and hence assumption (i) does not affect our arguments. But we note that the fact that the current samples of SMBHs have been discovered as quasars indicates that they are accreting mass almost at maximum efficiency, at least at the time when they were observed (i.e., $z \sim 6$). Indeed the quasar (CEERS_1019) with the BH whose mass is $\sim 10^7 M_{\odot}$ at $z = 8.679$ was recently found by the Cosmic Evolution Early Release Science survey with the James Webb Space Telescope [17], which gives interesting implications for the growth scenario of SMBHs.

As this equation shows, the PBH correlation function is determined by two quantities ν and $\epsilon(r)$, which we explain below one by one. First, the dimensionless quantity ν is the measure of rareness of the PBHs: only locations where the random Gaussian scalar field which is a source of PBHs takes a value greater than $\nu\sigma$ (σ^2 is the variance of the scalar field fluctuations) collapse to PBHs after inflation. It is related to the abundance of the observed number density of quasars by

$$\frac{e^{-\nu^2/2}}{\sqrt{2\pi\nu}} \sim 4 \times 10^{-12} f \left(\frac{M_{\text{PBH}}}{10^{10} M_{\odot}}\right)^{3/2} \left(\frac{n_{\text{QSO}}}{40 \text{ Gpc}^{-3}}\right), \quad (2.4)$$

where n_{QSO} is the average (comoving) number density of observed quasars (QSOs). We also consider the possibility that PBHs constitute only a fraction of quasars, and f represents the fraction of PBHs in quasars, which is defined as $f \equiv n_{\text{PBH}}/n_{\text{QSO}}$ where n_{PBH} is the average number density of PBHs. We have taken $n_{\text{QSO}} = 40 \text{ Gpc}^{-3}$ as a fiducial value based on [45].⁷ Notice that the right-hand side of the above equation is extremely small even if $f = 1$ and, hence, $\nu \gg 1$ always holds. This shows that PBHs are sparsely populated at their formation epoch.

Second, the function $\epsilon(r)$ is the normalized two-point function of the spectator field fluctuations produced during inflation:

$$\epsilon(r) = \frac{c_I}{k_{\text{max}}^{c_I} - k_{\text{min}}^{c_I}} \int_{k_{\text{min}}}^{k_{\text{max}}} \frac{dk}{k} k^{c_I} \frac{\sin(kr)}{kr}, \quad c_I = \frac{2m^2}{3H_I^2}. \quad (2.5)$$

Here m and H_I denote a mass of the spectator field and the Hubble parameter during inflation, respectively. The minimum comoving wave number, k_{min} , defines the size of the observable region in which our perturbation is defined. Thus, we take $k_{\text{min}} = H_0$ with H_0 being the Hubble parameter at the present epoch. The maximum wave number k_{max} is related to the PBH mass by Eq. (2.1) with the left-hand side replaced with k_{max} . k_{max} is determined by concrete inflationary models describing how the scalar field fluctuations are converted into primordial curvature perturbations that source PBHs. Since we want our present analysis to be general and independent of concrete models, we leave k_{max} (or equivalently M_{PBH}) as well as c_I and f as free parameters.

To summarize, the PBH angular correlation function depends on three quantities (M_{PBH}, c_I, f) that are free parameters in our models. We show the angular correlation function in models with PBHs for several values of M_{PBH} and c_I in Fig. 1. When $f < 1$, the angular correlation function of SMBHs is given by a sum of the angular

⁷We have used the luminosity function given by Eq. (8) in [45] and integrated it in the magnitude range $M_{1450} < -22.25$ assuming all the quasars are at $z = 6$.

correlation function of SMBHs of astrophysical origin, astrophysical black holes (ABHs), and that of PBHs:

$$\omega = \omega_{\text{ABH}} + \omega_{\text{PBH}} = (1 - f)^2 w_{\text{ABH}} + f^2 w_{\text{PBH}}, \quad (2.6)$$

where w_{ABH} is the angular correlation function predicted for SMBHs formed by astrophysical processes. Actually we need to consider four populations for SMBHs: active PBHs, nonactive PBHs, active astrophysical BHs and nonactive astrophysical BHs, where ‘‘active’’ indicates PBHs or BHs with the mass accreting with $M_{1450} < -22$ mag.⁸ Active populations are expected to be located at more biased places in the dark matter structure where mass accretion is more frequent. However, in the following argument, we assume that the clustering property we measure represents the whole PBHs + astrophysical BHs. Since the masses of SHELLQs and Sloan Digital Sky Survey quasars M_{BH} are distributed within 2 dex at most (see, e.g., [47] where the BH masses of high- z quasar ranges from $10^{7.6} M_{\odot}$ to $10^{9.3} M_{\odot}$), the difference in the clustering strength between quasars and non-quasar galaxies should not be huge. Therefore the quasar samples we used in our analysis are considered to represent more or less the whole population with similar accretion.

In this paper, we compare this angular correlation function with the distribution of the observed quasars on the sky and derive an allowed region in the parameter space spanned by (M_{PBH}, c_I, f) . For ω_{ABH} , we do not specify its explicit form in the following analysis since no definite prediction is available. However we note that ω_{ABH} based on Lyman break galaxies (LBGs) at high redshift has been obtained [48], which can be considered as a lower limit of ω_{ABH} . This is because, since the number of the entire LBG population is dominated by fainter LBGs which have lower stellar mass, the BH mass of LBGs should have systematically lower ones that of SHELLQs quasars.

III. QUASAR SAMPLE AND CLUSTERING ANALYSIS

A. Sample of $z \sim 6$ quasars

In order to evaluate the ACF of the quasars at $z \sim 6$ with the projected two-point angular correlation function, we use the quasar sample constructed by Matsuoka *et al.* (SHELLQs) [42]. It contains 81 quasars covering a wide magnitude range of $-25.58 \leq M_{1450} \leq -22.25$ at $5.88 \leq z \leq 6.49$, selected from the HSC-SSP PDR3 wide-layer dataset with a sky coverage of ~ 1200 deg² [49]. Additionally, to increase sample size, we include 11 known quasars [8,50–58] falling within the sky coverage of the wide-layer dataset in the same redshift range. Distributions of redshift and UV absolute magnitude of the quasar sample are plotted in the left and right panel of Fig. 2, respectively.

⁸In [46], it is argued that the observed quasars may occupy a small fraction of the total SMBHs seeded by galaxies.

The two-point correlation function is estimated by comparing the number of pairs of real quasars and that of randomly distributed mock quasars in the survey area. We construct the sample of random quasars as follows. HSC-SSP PDR3 provides a catalog of random points with a density of 100 points per arcmin² for each coadd image for each filter [49,59]. To mask regions with unreliable photometry, we apply the same criteria used to select the real quasars to the random catalog:

$$\begin{aligned} \text{pixelflags_edge} &= \text{False}, \\ \text{pixelflags_saturatedcenter} &= \text{False}, \\ \text{pixelflags_crcenter} &= \text{False}, \\ \text{pixelflags_bad} &= \text{False}, \\ \text{isprimary} &= \text{True}, \end{aligned}$$

in the izy bands, and

$$\text{inputcount_value} \geq 2$$

in the z_{AB} band. In addition, we apply the following criteria to mask regions around bright sources,

$$\begin{aligned} \text{mask_brightstar_halo} &= \text{False}, \\ \text{mask_brightstar_ghost} &= \text{False}, \\ \text{mask_brightstar_blooming} &= \text{False}, \end{aligned}$$

in the izy bands, and

$$\text{mask_brightstar_channel_stop} = \text{False}$$

in the y_{AB} band. Then we randomly select 1,00,000 points.

We note that the detection limit does not uniformly distribute over the sky coverage of the wide-layer dataset, as PDR3 only includes data obtained by January 2020, and the detection limit can be affected by nonuniform seeing. Since the nonuniform distribution of detection limits can affect the selection of real quasars, it is necessary to reproduce this nonuniform distribution in the random quasars as well. We consider this effect as follows. First, we examine the relation between magnitude errors and magnitudes in the z band of real point sources on the wide-layer dataset. We adopt the criteria used in [45], $z_{\text{psf,AB}} - z_{\text{CModel,AB}} < 0.15$ where $z_{\text{CModel,AB}}$ is the CModel magnitude [60] to select point sources, and found that patch (2,3) of tract 9567 includes 126 point sources, which are abundant enough for the analysis.⁹ An exponential function is applied to fit magnitude errors in the z band of the real point sources on the patch as a function of their z -band magnitudes. The best-fit model is plotted by red line in Fig. 3. Then, we shift the best-fit model to match the five-sigma detection limit in the z band for each patch, and

⁹Tract is a 1.7×1.7 degree region, and each tract is divided into 9×9 patches.

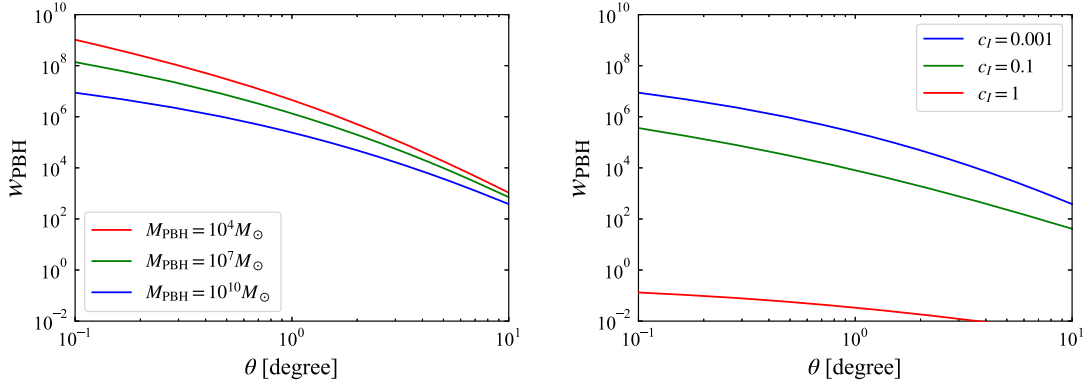


FIG. 1. The dependency of the PBH angular correlation function on the PBH mass when $c_l = 0.001$ (left panel) and the scalar field mass when $M_{\text{PBH}} = 10^{10} M_\odot$ (right panel). In both cases, the integral to the line of sight was performed setting $(z_{\text{low}}, z_{\text{high}}) = (5.88, 6.5)$.

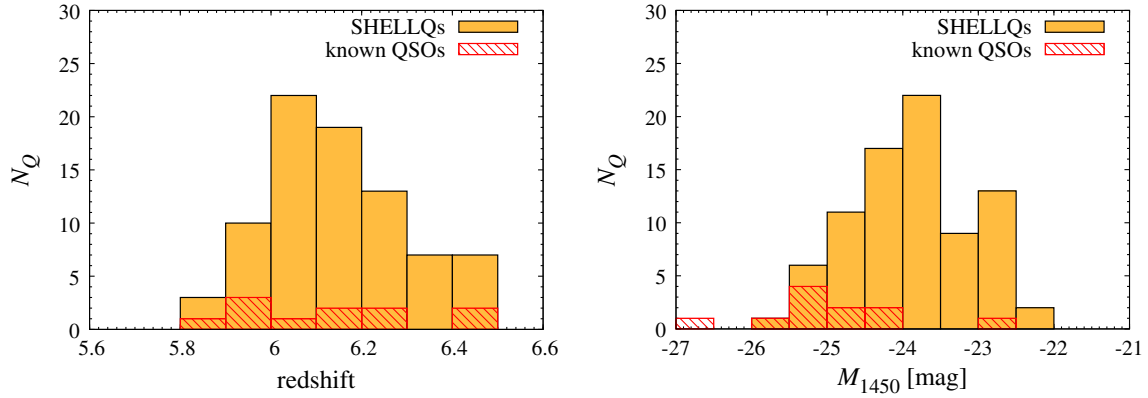


FIG. 2. Distributions of redshift (left) and UV absolute magnitude M_{1450} (right) of quasars we adopt in our analysis.

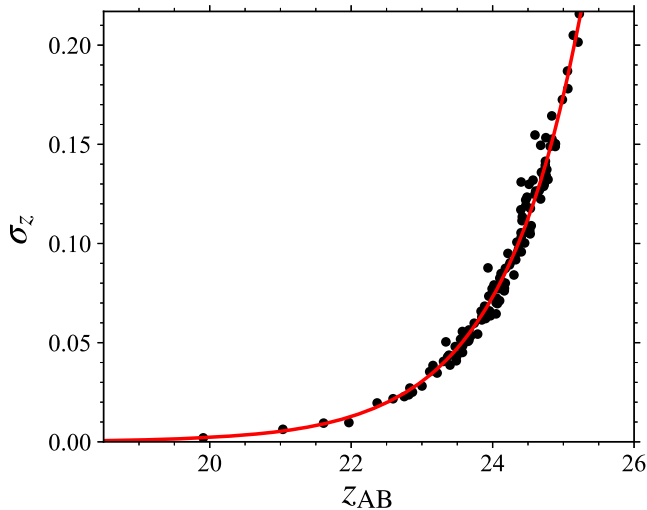


FIG. 3. Relations between the z -band photometric uncertainty and z -band magnitude. Dots represent point sources on patch (2,3) of tract 9567 of HSC PDR3 wide imaging. The red line shows the fitting formula, $\sigma_z = a \exp(b z_{\text{AB}})$ where $a = (6.03 \pm 2.26) \times 10^{-11}$ and $b = 0.87 \pm 0.02$.

assign the corresponding magnitude error at $z_{\text{AB}} = 24.5$ to each random position falling in the patch. Finally, we adopt the criterion in the z -band magnitude error $\sigma_z < 0.155$, which is used to select the real quasars, to the random positions criteria [42].

In total, we obtain 87,933 random positions, and we regard them as random quasars hereafter. Figure 4 shows the cumulative distribution functions of the depth in the z band for random and real quasars. Although there are small discrepancies at the depth around 24.8 and 25.6 mag, given the fraction of affected patches are limited, both distributions are considered to be consistent, i.e., the random quasars are properly generated. We confirmed that the size of random quasars is sufficient for the clustering analysis as more random quasars do not significantly change the derived angular correlation function.

B. Angular correlation function of $z \sim 6$ quasars

To derive the angular correlation function ω with $z \sim 6$ quasars, we adopt the estimator given by Davis and Peebles [61]:

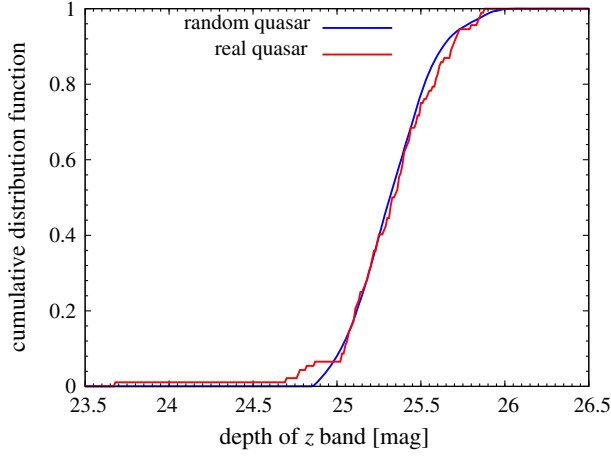


FIG. 4. Cumulative distributions of the z -band detection depth at the patch of the real (red) and random (blue) quasars.

$$\omega(\theta) = \frac{DD(\theta)}{DR(\theta)} - 1, \quad (3.1)$$

where DD and DR are the normalized counts of the quasar-quasar and quasar-random pairs between $\theta - \Delta\theta$ and $\theta + \Delta\theta$, and they are given by

$$DD(\theta) = \frac{N_{QQ}(\theta)}{N_Q(N_Q - 1)/2}, \quad DR(\theta) = \frac{N_{QR}(\theta)}{N_Q N_R}. \quad (3.2)$$

Here, N_{QQ} and N_{QR} are the numbers of the quasar-quasar and quasar-random pairs in the each bin, and N_Q and N_R are the total counts of the real and random quasars, respectively. We count the number of DD or DR pairs in 12 logarithmically spaced bins in the angular scale of $0.2 < \theta/\text{deg} < 10$.

We evaluate the uncertainty of ACF by the Jackknife resampling [62]. We separate the entire survey area into 10 subregions. In each resampling, we exclude one subregion, and estimate the ACF for the real and random quasars on the remaining regions with the same estimator described above. The uncertainty of the ACF is evaluated by the diagonal elements of the covariance matrix:

$$C_{ij} = \frac{N-1}{N} \sum_{k=1}^N (\omega_i^k - \bar{\omega}_i)(\omega_j^k - \bar{\omega}_j), \quad (3.3)$$

where $\bar{\omega}_i$ is the average of the angular correlation function for 10 estimates. We regard the square root of the diagonal elements C_{ii} as the uncertainty for the i th bin, i.e., $\sigma_{JK,i} \equiv \sqrt{C_{ii}}$. The resulting ACF and its uncertainty for each bin are plotted in Fig. 5, and summarized in Table I.

We fit the derived ACF with power-law function:

$$\omega_{\text{fit}}(\theta) = A_\omega \left(\frac{\theta}{\text{deg}} \right)^{-\beta}. \quad (3.4)$$

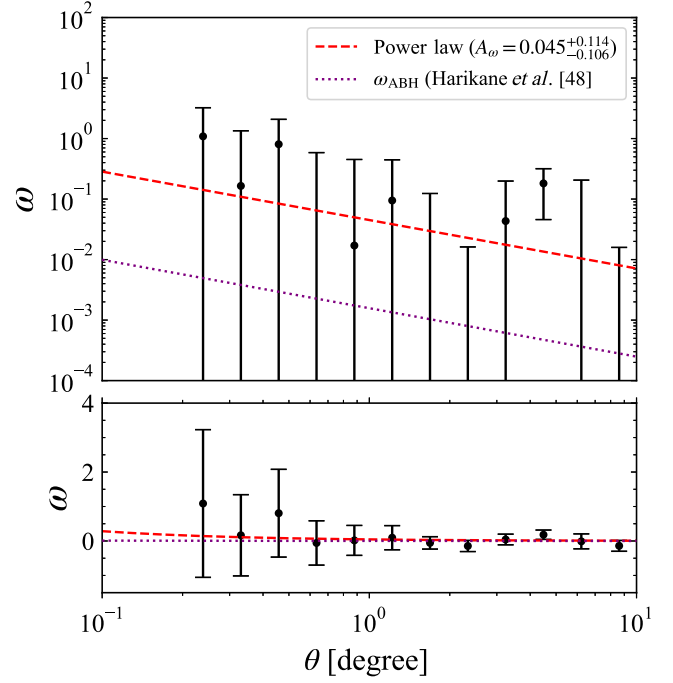


FIG. 5. Two-point angular autocorrelation function derived with $z \sim 6$ quasars (black dot) in the logarithmic (upper panel) and linear (bottom panel) scales. The best-fit power-law model is shown by red dashed line. For comparison, we also display the ACF of LBGs down to $m_{UV} = 28.4$ at $z \sim 6$ [48] by purple dotted line.

Due to the limited size of quasar samples used in the analysis, we fix the power index β to 0.8 to reduce the number of free parameters in the fitting. The chosen power index is determined by the ACFs of galaxies in the lower redshifts [48,63–67]. We carry out the fitting through the maximum likelihood method [68] (see also [69]), which is less affected by negative bins compared to the χ^2 fitting method, since the former method does not require a specific binning.

We define the likelihood \mathcal{L} of having the observed pair sample against the model prediction under the assumption that the pair count in each bin follows the Poisson distribution as follows [68]:

$$\mathcal{L} \equiv \prod_{i=1}^{\text{all bins}} \frac{e^{-h(\theta_i)} [h(\theta_i)]^{N_{QQ}(\theta_i)}}{[N_{QQ}(\theta_i)]!}, \quad (3.5)$$

where $h_i \equiv (1 + w_i)DR_i$ is the expected quasar-quasar pair count estimated by the quasar-random pair counts within the small interval around θ . The free parameter A_ω is determined by minimizing $S \equiv -2 \ln \mathcal{L}$ which is explicitly given by

$$S = 2 \sum_i^{\text{all bins}} h(\theta_i) - 2 \sum_i^{\text{all bins}} N_{QQ}(\theta_i) \ln h(\theta_i). \quad (3.6)$$

TABLE I. ACF of $z \sim 6$ quasars.

No.	θ [deg]	$(\theta - \Delta\theta, \theta + \Delta\theta)$ [deg]	N_{QQ}	N_{QR}	ω	σ_{JK}
1	0.24	(0.2, 0.28)	1	926	1.087	2.143
2	0.33	(0.28, 0.38)	1	1659	0.165	1.178
3	0.46	(0.38, 0.53)	3	3211	0.806	1.273
4	0.63	(0.53, 0.74)	3	6151	-0.057	0.643
5	0.88	(0.74, 1.02)	6	11401	0.017	0.434
6	1.22	(1.02, 1.41)	12	21185	0.095	0.350
7	1.69	(1.41, 1.96)	19	38889	-0.056	0.179
8	2.34	(1.96, 2.71)	30	67589	-0.146	0.162
9	3.24	(2.71, 3.76)	59	109289	0.043	0.155
10	4.49	(3.76, 5.21)	96	157019	0.181	0.136
11	6.21	(5.21, 7.22)	104	203253	-0.011	0.217
12	8.61	(7.22, 10.0)	108	242998	-0.141	0.157

If we assume S follows the χ^2 distribution, then the 1σ uncertainty of the best-fit A_ω can be evaluated by the range with $\Delta S = S - S_{\min}$ less than one. The resulting best-fit A_ω is $0.045^{+0.114}_{-0.106}$, and the best-fit power law model is plotted by red dashed line in Fig. 5. Arita *et al.* [70] have also studied the ACF of quasars at $z \sim 6$ using data from the SHELLQs project.¹⁰ Here we comment on the comparison between that derived by Arita *et al.* and us. Their quasar sample excluded type-2 AGN candidates and the final sample consists of 107 quasars with a luminosity range of $-27.0 < M_{1450} < -21.3$. While there were slight differences between their sample and ours, and they adopted a different estimator from Landy and Szalay [71] to calculate the ACF, we found that the best-fit power-law model of the ACF of quasars at $z \sim 6$ is consistent between the two studies.

IV. TESTING THE PBH SCENARIO AS SMBHS

Now we discuss constraints on the PBH scenario as SMBHS using the angular correlation function obtained from SHELLQs quasar data. Figure 6 shows 2σ constraints on the PBH parameters c_I and f for different values of $M_{\text{PBH}} = 10^4 M_\odot$, $10^7 M_\odot$, and $10^{10} M_\odot$. We judge that a model is allowed when it predicts the ACF consistent with the observed ACF within 2σ error for all bins. White region in each panel is the allowed one consistent with the SHELLQs data and the left region from red curve (shaded with colors) is ruled out. To obtain the constraints, we neglect the contribution from ω_{ABH} , which gives a conservative limit on the PBH parameters. In particular, by rewriting Eq. (2.6) as $f^2 \omega_{\text{PBH}} = \omega_{\text{obs}} - (1-f)^2 \omega_{\text{ABH}}$ with ω_{obs} being the observed ACF, one can easily notice that any contribution from ABH (i.e., assuming $\omega_{\text{ABH}} \neq 0$) always make the upper limit on the PBH abundance f smaller (tighter). We also show contours of the value of ω_{ref}

¹⁰Arita *et al.* [70] performed the analysis independently from this work.

predicted by the PBH model at the minimum angular scale among 12 bins, i.e., $\omega_{\text{ref}} \equiv \omega(0.24^\circ)$.

From this result, we can emphasize two important points: first, three panels look similar, which means that our constraint is only weakly dependent on M_{PBH} . This can be understood from the left panel of Fig. 1 which shows that, compared to the right panel of Fig. 1, the PBH angular correlation function does not change significantly as we vary M_{PBH} by several orders of magnitude. Although it is still uncertain that how much the PBHs can grow their masses through accretion which may occur until PBHs are formed at high redshifts, our constraint on the PBH scenario as the origin of the SMBHS at high redshifts is rather insensitive to such an uncertainty. Second, the possibility that PBHs comprise all the observed SMBHS is completely ruled out except the case where c_I is close to 1. Especially, the contribution of PBHs is severely restricted to be $f \lesssim 10^{-4}$ for the case where the scalar field is nearly massless ($c_I \ll 1$). This is consistent with a crude estimate obtained by requiring that the angular correlation function of PBHs at the observationally relevant angular scales $\omega_{\text{PBH}} \sim 10^8$ (see Fig. 1) should not exceed the observed values $\omega_{\text{obs}} \sim 0.1$ (see Fig. 5): $f \lesssim \sqrt{\frac{\omega_{\text{obs}}}{\omega_{\text{PBH}}}} = \mathcal{O}(10^{-4})$.

Our result suggests that the PBH models to explain the SMBHS at high redshifts from non-Gaussian fluctuations generated by Gaussian fluctuations of nearly massless spectator field are incompatible with the observed spatial distribution of the SMBHS. Since this conclusion essentially comes from the property of the spectator field fluctuations that the locations of rare peaks of the field fluctuations, which are nothing but the locations of PBHs, are strongly clustered, our constraint does not rely on the concrete mechanism to convert the spectator field fluctuations to the primordial curvature perturbations. Thus, our conclusion can be applied to any PBH models as long as Gaussian fluctuations of a nearly massless spectator field give the seeds of PBH formation.

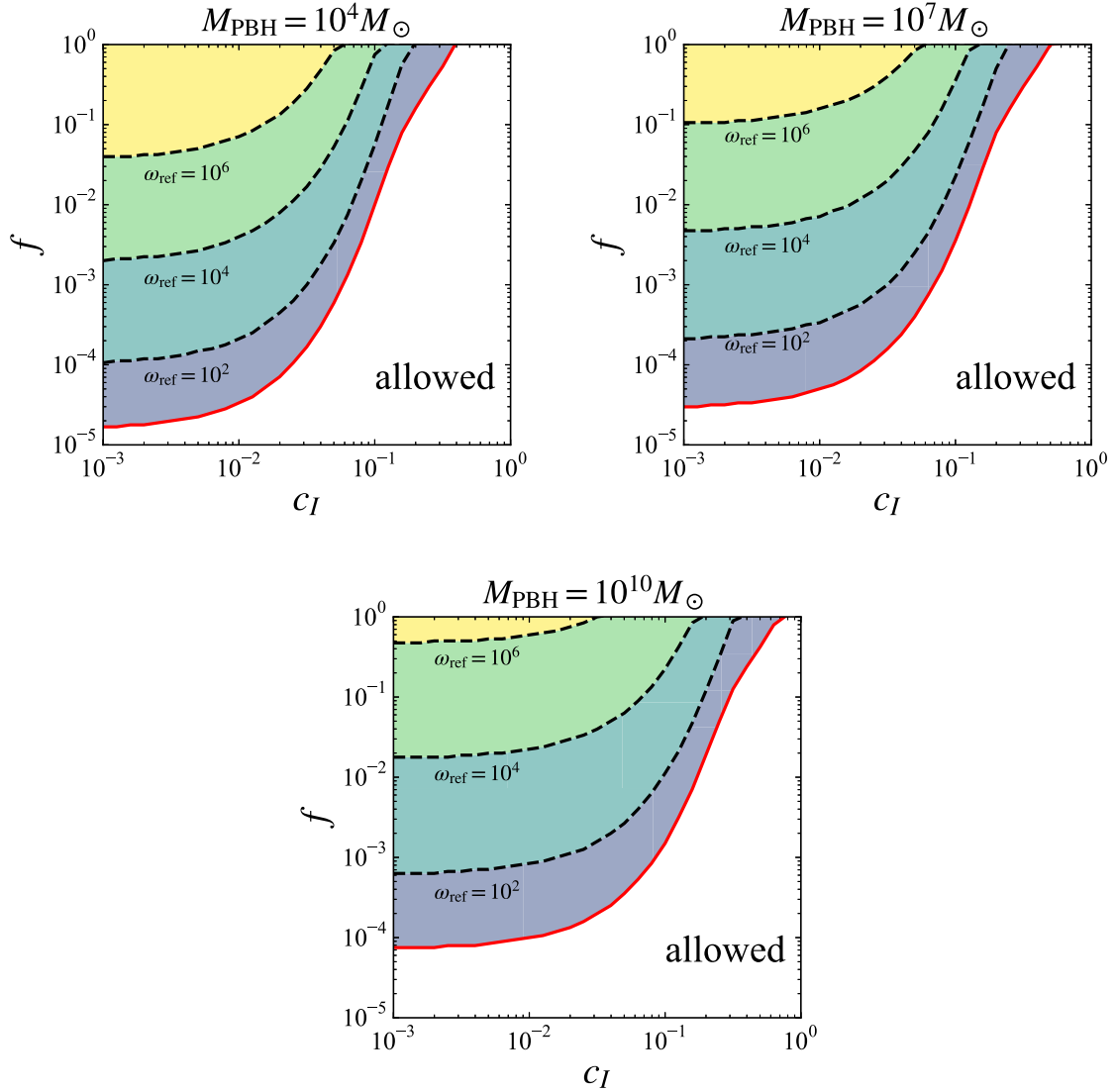


FIG. 6. Constraint from the angular correlation function derived from SHELLQs quasar data on the $c_l - f$ plane. White region is allowed from the requirement that $\omega_{\text{PBH}} < \omega_{\text{obs}}$ at 2σ in all bins. Cases with $M_{\text{PBH}} = 10^4 M_\odot$ (top left panel), $10^7 M_\odot$ (top right panel), and $10^{10} M_\odot$ (bottom panel) are shown. The dashed lines show the value of ω_{ref} predicted by the PBH model at the minimum angular scale among 12 bins, i.e., $\omega_{\text{ref}} \equiv \omega(0.24^\circ)$.

On the other hand, the white region in each panel of Fig. 6 is currently consistent with observations. A PBH scenario is still viable if the mass of the spectator field is comparable to the Hubble parameter during inflation. The constraint would get severer by reducing the error bars of the measurements of the angular correlation function of high- z SMBHs. This will be achieved in future by detecting more number of quasars. We will discover more than 200 quasars at $z > 6$ in total when the SHELLQs is completed. A significantly larger number of high- z quasars would be discovered in future projects, such as Rubin's Legacy Survey of Space and Time (LSST) [72]. Besides, a quasar at $z > 8$ has already been found by James Webb Space Telescope [17], and more samples at higher redshift are expected to be observed in the future. It should also be

noted that our analysis of SHELLQs data provides a hint that the observed angular correlation function is nonzero. If the angular correlation function is actually nonzero, the models predicting the Poisson distribution of PBHs are ruled out. For instance, the PBHs originating from the vacuum bubbles produced by quantum tunneling during inflation [36] are not compatible with observations if the tunneling rate depends only on the adiabatic direction (see footnote 3). These considerations suggest that further reduction of the measurement errors of the angular correlation function by using a greater number of quasars in the future is crucial to test the possibility of PBHs as the origin of the observed SMBHs at high redshifts.

Before closing this section, let us mention that our result also severely constrains our PBH model using the spectator

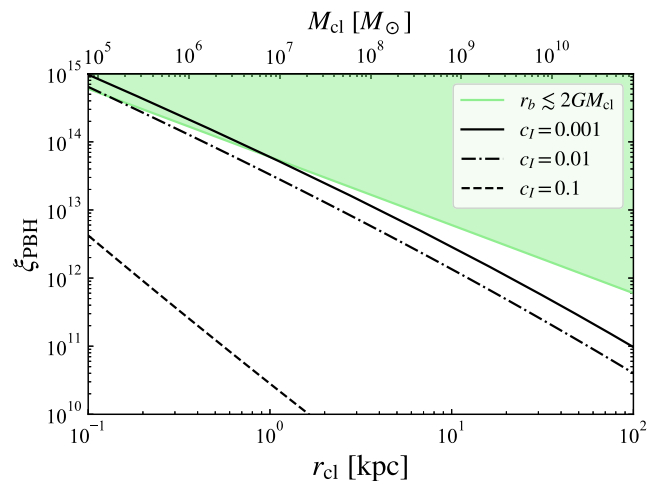


FIG. 7. The PBH correlation function in the scenario that PBH clump collapses into SMBH. The green line is the lower bound given from the condition that the clump radius r_b is shorter than the Schwarzschild radius.

field in the context of an alternative scenario [73] in which SMBHs at high redshifts originate from the direct collapse of PBH clumps containing many smaller PBHs. In this scenario, the initial PBH number density inside a clump is so large that the clump directly turns into a much heavier BH soon after the clump decouples from the Hubble expansion in deep radiation dominated era as is the case in the standard PBH formation in which overdense region with large amplitude decouples from the Hubble expansion soon after the horizon reentry and collapses to a BH. At the level of the order-of-magnitude estimate, the direct collapse of the PBH clump is achieved if the physical size of the clump at the time of the decoupling is less than the Schwarzschild radius of the clump, which we use as the criterion for the direct collapse. As a concrete example, the green line in Fig. 7 represents the boundary of the criterion in the case where $M_{\text{PBH}} = M_{\odot}$ and $f_{\text{PBH}} = 10^{-9}$.¹¹ The direct collapse occurs in the region above the green line. The horizontal and vertical axes are the comoving radius of the clumps and the magnitude of the two-point correlation function, respectively. Upper horizontal axis represents the masses of the resultant heavier BHs originating from clumps. As we can verify, ξ_{PBH} intersects with the green line at $r_{\text{cl}} \sim 1$ kpc if c_I is sufficiently small ($c_I \lesssim 0.01$). The mass of the resultant heavier BHs is $\approx 10^7 M_{\odot}$. This magnitude is large enough to explain the origin of the SMBHs observed at high redshifts without resorting to the efficient mass growth due to accretion after the formation of the heavier BHs. However, as we see in the figure, in such cases, the magnitude

¹¹In [73], the redshift when the decoupling of the clump from the Hubble expansion occurs is fixed to $z_{\text{eq}}/\xi_{\text{PBH}}$, where z_{eq} is the redshift at the matter-radiation equality. On the other hand, the green line in Fig. 7 is obtained by adopting $z_{\text{eq}}/(\xi_{\text{PBH}} f_{\text{PBH}})$ as the redshift of decoupling.

of the correlation function at length scales corresponding to the quasar measurements largely exceeds the measured correlation function obtained in this paper from the quasar measurements. Thus, the scenario proposed in [73] in the context of our PBH model is incompatible with the measured quasar distribution on the sky and cannot be considered to be viable.

V. CONCLUSION

We derived the angular correlation function by using 92 quasars at $z \sim 6$ observed by SHELLQs, and the result is shown in Fig. 5. We fitted the derived ACF to the power-law function (3.4) and obtained its best-fit model as $A_{\omega} = 0.045^{+0.114}_{-0.106}$. Then we compared the angular correlation functions from SHELLQs with the theoretically predicted ones from the PBH model, which can serve as a critical test for the PBH SMBH scenarios.

Theoretical predictions for the angular correlation function of PBHs have been given in [37] for a general scenario where Gaussian fluctuations of the spectator field result in highly non-Gaussian curvature perturbation and the perturbation collapses into PBH. Such a PBH scenario can explain SMBHs while avoiding the constraint from the CMB μ distortion. According to [37], a very high clustering of PBHs occurs as long as the mass of the spectator field is sufficiently small. However, when the mass gets close to the Hubble parameter during inflation, the size of the angular correlation function becomes smaller (see the right panel of Fig. 1). In addition, given that observed quasars may be a combination of PBH and astrophysical ones, we introduced the fraction of PBH-origin SMBHs f as an extra parameter. Then we placed a limit on these parameters c_I and f by comparing to the correlation function derived from $z \sim 6$ quasars observed by SHELLQs [42].

In Fig. 6, the constraint in the $c_I - f$ plane is depicted for several values of PBH masses. From the figure, we can see that the result is almost independent of the PBH mass M_{PBH} . Our result indicates that the PBH scenario as SMBHs is excluded when the mass of the spectator field is sufficiently smaller than the Hubble rate during inflation. We note that the astrophysical contribution ω_{ABH} is neglected in our analysis, but this gives conservative constraints on the PBH parameters. In other words, if we include the astrophysical contribution in our analysis, the contribution of ω_{PBH} allowed by the observation should be smaller compared to the present case and the excluded regions in Fig. 6 would be broadened. If more high- z quasars are discovered in the future, the measurement error will be reduced, and more accurate constraints will be obtained.

We also discussed a scenario where clumps of PBHs in early time collapses into SMBHs or its seeds. Following the method of [73], we found that if the spectator field is very light ($c_I \ll 1$), the creation of the seed of SMBHs at high- z would be possible as shown in Fig. 7. However, the correlation function in that case is much larger than the

one we derived from SHELLQs quasars at $z \sim 6$, and hence such a scenario is also prohibited.

Finally we emphasize again that our result indicates that the PBH scenarios based on the spectator field as the origin of SMBHs at $z \sim 6$ are almost excluded for a wide range of parameter space. This may indicate that SMBHs are of astrophysical origin unless an alternative cosmological model is suggested.

ACKNOWLEDGMENTS

We are grateful to Nobunari Kashikawa and Junya Arita for helpful and fruitful discussions. We also thank Taira Oogi for the communication on theoretical predictions of the angular correlation function for high- z quasars. This work is supported in part by the MEXT KAKENHI Grants No. 17H06359 (T.S.), No. JP21H05453 (T.S.), and the JSPS KAKENHI Grants No. JP17H04830 (Y.M.), No. 21H04494 (Y.M.), No. 20H01949 (T.N.), No. 23H01215 (T.N.), No. JP19K03864 (T.S.) and No. 19K03874 (T.T.). The Hyper Suprime-Cam (HSC) collaboration includes the astronomical communities of Japan and Taiwan, and Princeton University. The HSC

instrumentation and software were developed by NAOJ, the Kavli Institute for the Physics and Mathematics of the Universe (Kavli IPMU), the University of Tokyo, the High Energy Accelerator Research Organization (KEK), the Academia Sinica Institute for Astronomy and Astrophysics in Taiwan (ASIAA), and Princeton University. Funding was contributed by the FIRST program from Japanese Cabinet Office, MEXT, JSPS, Japan Science and Technology Agency (JST), the Toray Science Foundation, NAOJ, Kavli IPMU, KEK, ASIAA, and Princeton University. This paper is based on data collected at the Subaru Telescope and retrieved from the HSC data archive system, which is operated by Subaru Telescope and Astronomy Data Center (ADC) at NAOJ. Data analysis was in part carried out with the cooperation of Center for Computational Astrophysics (CfCA) at NAOJ. We are honored and grateful for the opportunity of observing the Universe from Maunakea, which has cultural, historical, and natural significance in Hawaii. This paper makes use of software developed for Vera C. Rubin Observatory. We thank the Rubin Observatory for making their code available as free software at [74].

-
- [1] X. Fan *et al.*, A survey of $z > 5.8$ quasars in the Sloan digital sky survey. I. Discovery of three new quasars and the spatial density of luminous quasars at $z \sim 6$, *Astron. J.* **122**, 2833 (2001).
- [2] L. Jiang, I. D. McGreer, X. Fan, M. A. Strauss, E. Bañados, R. H. Becker, F. Bian, K. Farnsworth, Y. Shen, F. Wang, R. Wang, S. Wang, R. L. White, J. Wu, X.-B. Wu, J. Yang, and Q. Yang, The final SDSS high-redshift quasar sample of 52 quasars at $z > 5.7$, *Astrophys. J.* **833**, 222 (2016).
- [3] Y. Matsuoka *et al.*, Subaru high- z exploration of low-luminosity quasars (SHELLQs). I. Discovery of 15 quasars and bright galaxies at $5.7 < z < 6.9$, *Astrophys. J.* **828**, 26 (2016).
- [4] Y. Matsuoka *et al.*, Discovery of the first low-luminosity quasar at $z > 7$, *Astrophys. J. Lett.* **872**, L2 (2019).
- [5] Y. Matsuoka *et al.*, Subaru high- z exploration of low-luminosity quasars (SHELLQs). XVI. 69 new quasars at $5.8 < z < 7.0$, *Astrophys. J. Suppl. Ser.* **259**, 18 (2022).
- [6] C. J. Willott, P. Delorme, A. Omont, J. Bergeron, X. Delfosse, T. Forveille, L. Albert, C. Reylé, G. J. Hill, M. Gully-Santiago, P. Vinten, D. Crampton, J. B. Hutchings, D. Schade, L. Simard, M. Sawicki, A. Beelen, and P. Cox, Four quasars above redshift 6 discovered by the Canada-France high- z quasar survey, *Astron. J.* **134**, 2435 (2007).
- [7] C. J. Willott, P. Delorme, C. Reylé, L. Albert, J. Bergeron, D. Crampton, X. Delfosse, T. Forveille, J. B. Hutchings, R. J. McLure, A. Omont, and D. Schade, The Canada-France high- z quasar survey: Nine new quasars and the luminosity function at redshift 6, *Astron. J.* **139**, 906 (2010).
- [8] E. Bañados *et al.*, The pan-STARRS1 distant $z > 5.6$ quasar survey: More than 100 quasars within the first Gyr of the universe, *Astrophys. J. Suppl. Ser.* **227**, 11 (2016).
- [9] D. J. Mortlock, S. J. Warren, B. P. Venemans, M. Patel, P. C. Hewett, R. G. McMahon, C. Simpson, T. Theuns, E. A. González-Solares, A. Adamson, S. Dye, N. C. Hambly, P. Hirst, M. J. Irwin, E. Kuiper, A. Lawrence, and H. J. A. Röttgering, A luminous quasar at a redshift of $z = 7.085$, *Nature (London)* **474**, 616 (2011).
- [10] X.-B. Wu, F. Wang, X. Fan, W. Yi, W. Zuo, F. Bian, L. Jiang, I. D. McGreer, R. Wang, J. Yang, Q. Yang, D. Thompson, and Y. Beletsky, An ultraluminous quasar with a twelve-billion-solar-mass black hole at redshift 6.30, *Nature (London)* **518**, 512 (2015).
- [11] M. Onoue, N. Kashikawa, Y. Matsuoka, N. Kato, T. Izumi, T. Nagao, M. A. Strauss, Y. Harikane, M. Imanishi, K. Ito, K. Iwasawa, T. Kawaguchi, C.-H. Lee, A. Noboriguchi, H. Suh, M. Tanaka, and Y. Toba, Subaru high- z exploration of low-luminosity quasars (SHELLQs). VI. Black hole mass measurements of six quasars at $6.1 \leq z \leq 6.7$, *Astrophys. J.* **880**, 77 (2019).
- [12] E. P. Farina *et al.*, The X-shooter/ALMA sample of quasars in the epoch of reionization. II. Black hole masses, Eddington ratios, and the formation of the first quasars, *Astrophys. J.* **941**, 106 (2022).

- [13] K. Inayoshi, E. Visbal, and Z. Haiman, The assembly of the first massive black holes, *Annu. Rev. Astron. Astrophys.* **58**, 27 (2020).
- [14] S. Hawking, Gravitationally collapsed objects of very low mass, *Mon. Not. R. Astron. Soc.* **152**, 75 (1971).
- [15] B. J. Carr and S. W. Hawking, Black holes in the early Universe, *Mon. Not. R. Astron. Soc.* **168**, 399 (1974).
- [16] B. J. Carr, The primordial black hole mass spectrum, *Astrophys. J.* **201**, 1 (1975).
- [17] G.-W. Yuan, L. Lei, Y.-Z. Wang, B. Wang, Y.-Y. Wang, C. Chen, Z.-Q. Shen, Y.-F. Cai, and Y.-Z. Fan, Rapidly growing primordial black holes as seeds of the massive high-redshift JWST galaxies, [arXiv:2303.09391](https://arxiv.org/abs/2303.09391).
- [18] B. Carr, K. Kohri, Y. Sendouda, and J. Yokoyama, Constraints on primordial black holes, *Rep. Prog. Phys.* **84**, 116902 (2021).
- [19] S. Bird, I. Cholis, J. B. Muñoz, Y. Ali-Haïmoud, M. Kamionkowski, E. D. Kovetz, A. Raccanelli, and A. G. Riess, Did LIGO Detect Dark Matter?, *Phys. Rev. Lett.* **116**, 201301 (2016).
- [20] S. Clesse and J. García-Bellido, The clustering of massive primordial black holes as dark matter: Measuring their mass distribution with Advanced LIGO, *Phys. Dark Universe* **15**, 142 (2017).
- [21] M. Sasaki, T. Suyama, T. Tanaka, and S. Yokoyama, Primordial Black Hole Scenario for the Gravitational-Wave Event GW150914, *Phys. Rev. Lett.* **117**, 061101 (2016); **121**, 059901(E) (2018).
- [22] S. Hirano, T. Hosokawa, N. Yoshida, H. Umeda, K. Omukai, G. Chiaki, and H. W. Yorke, One hundred first stars: Protostellar evolution and the final masses, *Astrophys. J.* **781**, 60 (2014).
- [23] J. L. Johnson and V. Bromm, The aftermath of the first stars: Massive black holes, *Mon. Not. R. Astron. Soc.* **374**, 1557 (2007).
- [24] B. D. Smith, J. A. Regan, T. P. Downes, M. L. Norman, B. W. O’Shea, and J. H. Wise, The growth of black holes from population III remnants in the renaissance simulations, *Mon. Not. R. Astron. Soc.* **480**, 3762 (2018).
- [25] L. Haemmerlé, L. Mayer, R. S. Klessen, T. Hosokawa, P. Madau, and V. Bromm, Formation of the first stars and black holes, *Space Sci. Rev.* **216**, 48 (2020).
- [26] T. Hosokawa, H. W. Yorke, K. Inayoshi, K. Omukai, and N. Yoshida, Formation of primordial supermassive stars by rapid mass accretion, *Astrophys. J.* **778**, 178 (2013).
- [27] T. E. Woods *et al.*, Titans of the early universe: The proto statement on the origin of the first supermassive black holes, *Pub. Astron. Soc. Aust.* **36**, e027 (2019).
- [28] L. Mayer, S. Kazantzidis, P. Madau, M. Colpi, T. R. Quinn, and J. Wadsley, Rapid formation of supermassive black hole binaries in galaxy mergers with gas, *Science* **316**, 1874 (2007).
- [29] N. Duechting, Supermassive black holes from primordial black hole seeds, *Phys. Rev. D* **70**, 064015 (2004).
- [30] M. Kawasaki, A. Kusenko, and T. T. Yanagida, Primordial seeds of supermassive black holes, *Phys. Lett. B* **711**, 1 (2012).
- [31] T. Nakama, T. Suyama, and J. Yokoyama, Supermassive black holes formed by direct collapse of inflationary perturbations, *Phys. Rev. D* **94**, 103522 (2016).
- [32] F. Hasegawa and M. Kawasaki, Cogenesis of LIGO primordial black holes and dark matter, *Phys. Rev. D* **98**, 043514 (2018).
- [33] M. Kawasaki and K. Murai, Formation of supermassive primordial black holes by Affleck-Dine mechanism, *Phys. Rev. D* **100**, 103521 (2019).
- [34] N. Kitajima and F. Takahashi, Primordial black holes from QCD axion bubbles, *J. Cosmol. Astropart. Phys.* **11** (2020) 060.
- [35] K. Kohri, T. Nakama, and T. Suyama, Testing scenarios of primordial black holes being the seeds of supermassive black holes by ultracompact minihalos and CMB μ -distortions, *Phys. Rev. D* **90**, 083514 (2014).
- [36] H. Deng and A. Vilenkin, Primordial black hole formation by vacuum bubbles, *J. Cosmol. Astropart. Phys.* **12** (2017) 044.
- [37] T. Shinohara, T. Suyama, and T. Takahashi, Angular correlation as a novel probe of supermassive primordial black holes, *Phys. Rev. D* **104**, 023526 (2021).
- [38] M. Kawasaki, K. Murai, and H. Nakatsuka, Strong clustering of primordial black holes from Affleck-Dine mechanism, *J. Cosmol. Astropart. Phys.* **10** (2021) 025.
- [39] Y. Tada and S. Yokoyama, Primordial black holes as biased tracers, *Phys. Rev. D* **91**, 123534 (2015).
- [40] S. Young and C. T. Byrnes, Signatures of non-Gaussianity in the isocurvature modes of primordial black hole dark matter, *J. Cosmol. Astropart. Phys.* **04** (2015) 034.
- [41] T. Suyama and S. Yokoyama, Clustering of primordial black holes with non-Gaussian initial fluctuations, *Prog. Theor. Exp. Phys.* **2019**, 103E02 (2019).
- [42] Y. Matsuoka *et al.*, Subaru high- z exploration of low-luminosity quasars (SHELLQs). XVI. 69 new quasars at $5.8 < z < 7.0$, *Astrophys. J. Suppl. Ser.* **259**, 18 (2022).
- [43] F. Hasegawa and M. Kawasaki, Primordial black holes from Affleck-Dine mechanism, *J. Cosmol. Astropart. Phys.* **01** (2019) 027.
- [44] N. Kaiser, On the Spatial correlations of Abell clusters, *Astrophys. J. Lett.* **284**, L9 (1984).
- [45] Y. Matsuoka *et al.*, Subaru high- z exploration of low-luminosity quasars (SHELLQs). V. Quasar luminosity function and contribution to cosmic reionization at $z = 6$, *Astrophys. J.* **869**, 150 (2018).
- [46] J. Buchner, E. Treister, F. E. Bauer, L. F. Sartori, and K. Schawinski, On the prevalence of supermassive black holes over cosmic time, *Astrophys. J.* **874**, 117 (2019).
- [47] M. Onoue, N. Kashikawa, Y. Matsuoka, N. Kato, T. Izumi, T. Nagao, M. A. Strauss, Y. Harikane, M. Imanishi, K. Ito *et al.*, Subaru high- z exploration of low-luminosity quasars (SHELLQs). VI. Black hole mass measurements of six quasars at $6.1 \leq z \leq 6.7$, *Astrophys. J.* **880**, 77 (2019).
- [48] Y. Harikane *et al.*, Evolution of stellar-to-halo mass ratio at $z = 0 - 7$ identified by clustering analysis with the Hubble legacy imaging and early Subaru/Hyper Suprime-Cam Survey data, *Astrophys. J.* **821**, 123 (2016).
- [49] H. Aihara *et al.*, Third data release of the Hyper Suprime-Cam Subaru Strategic Program, *Publ. Astron. Soc. Jpn.* **74**, 247 (2022).
- [50] C. J. Willott, A. Omont, and J. Bergeron, Redshift 6.4 host galaxies of 10^8 solar mass black holes: Low star formation rate and dynamical mass, *Astrophys. J.* **770**, 13 (2013).

- [51] C. J. Willott, P. Delorme, C. Reyl , L. Albert, J. Bergeron, D. Crampton, X. Delfosse, T. Forveille, J. B. Hutchings, R. J. McLure *et al.*, Six more quasars at redshift 6 discovered by the Canada–France high- z quasar survey, *Astron. J.* **137**, 3541 (2009).
- [52] L. Jiang, X. Fan, F. Bian, J. Annis, K. Chiu, S. Jester, H. Lin, R. H. Lupton, G. T. Richards, M. A. Strauss *et al.*, A survey of $z \sim 6$ quasars in the Sloan digital sky survey deep stripe. II. Discovery of six quasars at $z_{AB} > 21$, *Astron. J.* **138**, 305 (2009).
- [53] L.-H. Jiang *et al.*, A survey of $z \sim 6$ quasars in the SDSS deep stripe. I. A flux-limited sample at $z_{AB} < 21$, *Astron. J.* **135**, 1057 (2008).
- [54] C. Mazzucchelli, E. Ba ados, B. Venemans, R. Decarli, E. Farina, F. Walter, A.-C. Eilers, H.-W. Rix, R. Simcoe, D. Stern *et al.*, Physical properties of 15 quasars at $z \sim 6.5$, *Astrophys. J.* **849**, 91 (2017).
- [55] B. P. Venemans *et al.*, First discoveries of $z \sim 6$ quasars with the kilo-degree survey and VISTA kilo-degree infrared galaxy survey, *Mon. Not. R. Astron. Soc.* **453**, 2259 (2015).
- [56] Y. Kim, M. Im, Y. Jeon, M. Kim, C. Choi, J. Hong, M. Hyun, H. D. Jun, M. Karouzos, D. Kim *et al.*, Discovery of a faint quasar at $z \sim 6$ and implications for cosmic reionization, *Astrophys. J. Lett.* **813**, L35 (2015).
- [57] N. Kashikawa, Y. Ishizaki, C. J. Willott, M. Onoue, M. Im, H. Furusawa, J. Toshikawa, S. Ishikawa, Y. Niino, K. Shimasaku *et al.*, The Subaru high- z quasar survey: Discovery of faint $z \sim 6$ quasars, *Astrophys. J.* **798**, 28 (2014).
- [58] G. R. Zeimann, R. L. White, R. H. Becker, J. A. Hodge, S. A. Stanford, and G. T. Richards, Discovery of a radio-selected $z \sim 6$ quasar, *Astrophys. J.* **736**, 57 (2011).
- [59] H. Aihara *et al.*, Second data release of the Hyper Suprime-Cam Subaru Strategic Program, *Publ. Astron. Soc. Jpn.* **71**, 114 (2019).
- [60] J. Bosch, R. Armstrong, S. Bickerton, H. Furusawa, H. Ikeda, M. Koike, R. Lupton, S. Mineo, P. Price, T. Takata *et al.*, The hyper suprime-cam software pipeline, *Publ. Astron. Soc. Jpn.* **70**, S5 (2018).
- [61] M. Davis and P. J. E. Peebles, A survey of galaxy redshifts. 5. The two point position and velocity correlations, *Astrophys. J.* **267**, 465 (1982).
- [62] I. Zehavi *et al.* (SDSS Collaboration), The luminosity and color dependence of the galaxy correlation function, *Astrophys. J.* **630**, 1 (2005).
- [63] M. Ouchi, K. Shimasaku, H. Furusawa, T. Saito, M. Yoshida, M. Akiyama, Y. Ono, T. Yamada, K. Ota, N. Kashikawa *et al.*, Statistics of 207 *lya* emitters at a redshift near 7: Constraints on reionization and galaxy formation models, *Astrophys. J.* **723**, 869 (2010).
- [64] M. Ouchi *et al.*, Clustering properties of galaxies at $Z \sim 4$ in the Subaru/XMM deep survey field, *Astrophys. J. Lett.* **558**, L83 (2001).
- [65] M. Ouchi *et al.*, Subaru deep survey 6. A census of Lyman break galaxies at $z = 4$ and 5 in the Subaru deep fields: Clustering properties, *Astrophys. J.* **611**, 685 (2004).
- [66] S. Foucaud, H. J. McCracken, O. Le Fevre, S. Arnouts, M. Brodwin, S. J. Lilly, D. Crampton, and Y. Mellier, The Canada-France deep fields survey-2: Lyman—break galaxies and galaxy clustering at $Z \sim 3$, *Astron. Astrophys.* **409**, 835 (2003).
- [67] S. Foucaud, C. J. Conselice, W. G. Hartley, K. P. Lane, S. P. Bamford, O. Almaini, and K. Bundy, Clustering properties of galaxies selected in stellar mass: Breaking down the link between luminous and dark matter in massive galaxies from $z = 0$ to $z = 2$, *Mon. Not. R. Astron. Soc.* **406**, 147 (2010).
- [68] R. A. C. Croft, G. B. Dalton, G. Efstathiou, W. J. Sutherland, and S. J. Maddox, The richness dependence of galaxy cluster correlations: Results from a redshift survey of rich APM clusters, *Mon. Not. R. Astron. Soc.* **291**, 305 (1997).
- [69] W. He *et al.*, Clustering of quasars in a wide luminosity range at redshift 4 with Subaru Hyper Suprime-Cam wide field imaging, *Publ. Astron. Soc. Jpn.* **70**, S33 (2018).
- [70] J. Arita *et al.*, Subaru high- z exploration of low-luminosity quasars (SHELLQs) XVIII. The dark matter halo mass of quasars at $z \sim 6$, arXiv:2307.02531.
- [71] S. D. Landy and A. S. Szalay, Bias and variance of angular correlation functions, *Astrophys. J.* **412**, 64 (1993).
- [72] <https://www.lsst.org>.
- [73] V. De Luca, G. Franciolini, and A. Riotto, Clusteringgenesis: From Light to Heavy Primordial Black Holes, *Phys. Rev. Lett.* **130**, 171401 (2023).
- [74] <http://pipelines.lsst.io/>.